Spatial modes in one-dimensional models for capillary jets

J. Guerrero
Department of Chemistry and Physics, Georgia Regents University, 1120 15th Street, SCI W3005, Augusta, Georgia 30912, USA

H. González*
Departamento de Física Aplicada III, Escuela Técnica Superior de Ingeniería, Camino de los Descubrimientos, s/n, 41092-Sevilla, Spain

F. J. García
Departamento de Física Aplicada I, Escuela Politécnica Superior, Universidad de Sevilla, c/Virgen de África, 7, 41011-Sevilla, Spain
(Received 21 July 2015; published 7 March 2016)

One-dimensional (1D) models are widely employed to simplify the analysis of axisymmetric capillary jets. These models postulate that, for slender deformations of the free surface, the radial profile of the axial velocity can be approximated as uniform (viscous slice, averaged, and Cosserat models) or parabolic (parabolic model). In classical works on spatial stability analysis with 1D models, considerable misinterpretation was generated about the modes yielded by each model. The already existing physical analysis of three-dimensional (3D) axisymmetric spatial modes enables us to relate these 1D spatial modes to the exact 3D counterparts. To do so, we address the surface stimulation problem, which can be treated as linear, by considering the effect of normal and tangential stresses to perturb the jet. A Green's function for a spatially local stimulation having a harmonic time dependence provides the general formalism to describe any time-periodic stimulation. The Green's function of this signaling problem is known to be a superposition of the spatial modes, but in fact these modes are of fundamental nature, i.e., not restricted to the surface stimulation problem. The smallness of the wave number associated with each mode is the criterion to validate or invalidate the 1D approaches. The proposed axial-velocity profiles (planar or parabolic) also have a remarkable influence on the outcomes of each 1D model. We also compare with the classical 3D results for (i) conditions for absolute instability, and (ii) the amplitude of the unstable mode resulting from both normal and tangential surface stress stimulation. Incidentally, as a previous task, we need to re-deduce 1D models in order to include eventual stresses of various possible origins (electrohydrodynamic, thermocapillary, etc.) applied on the free surface, which were not considered in the previous general formulations.

DOI: 10.1103/PhysRevE.93.033102

I. INTRODUCTION

The analysis of capillary jets, such as that of many hydrodynamic systems with a free surface, is in general costly from a computational point of view. This was the reason for the early finding of simplifications, at least in the axisymmetric case [1,2]. The first widely accepted one-dimensional (1D) model was the *inviscid slice model* [3,4], in which both the axial velocity and the pressure at any normal section of the jet are considered as uniform. The next significant progress was the application of the *Cosserat model* [5,6]. Bogy [7] showed that this model gives better results in describing the dynamics of jets, particularly in the inviscid case. Eggers and Dupont [8] and García and Castellanos [9] generalized the inviscid slice model to the viscous case through a detailed deduction from the Navier-Stokes equations under the assumption of slender perturbations ($k \ll 1$, with k the wave number associated with the perturbation made dimensionless with the jet radius R) and an expansion of the velocity and pressure fields in the radial coordinate. We will call this improved model the *viscous slice model*. In the latter reference, other 1D models, namely, the *parabolic model* and the *averaged model*, were proposed. The parabolic model was so called because of an added quadratic term in the radial dependence of the axial velocity, thus requiring an additional function in the model formulation. As a counterpart to its higher computational cost, the parabolic model constitutes a k^4-order approximation, instead of the k^2-order approximation associated with the viscous slice model. Again in Ref. [9] the reader can find two novelties: (i) the rigorous deduction of the Cosserat model, showing its inconsistent retention of viscous terms that condemns it to k^2-order accuracy, and (ii) the proposal of the so-called averaged model, which cures the mentioned drawback of the Cosserat model, and has a k^4-order accuracy.

After its validation, 1D models have been extensively used as a tool to describe in an easier way the capillary jets subjected to a variety of physical effects, which can be classified in two types: (i) those acting in the bulk, such as gravity forces [10] and pressure modulation [11], and (ii) those acting on the free surface, such as surfactants [12], electric fields on conducting liquids [13–16], or thermocapillary forces [14,17]. For the latter type, 1D models needed specific adaptations to include the electrohydrodynamic (EHD) or thermocapillary surface stress terms considered for each particular case. In Sec. II we provide a general way to include surface stresses of any possible origin.

Although 1D models are originally nonlinear, many applications merely require linear versions of them, as the jet remains nearly cylindrical in most of its evolution until breakup. In the three-dimensional (3D) case, two classical descriptions of this linear evolution have been developed: the *temporal stability analysis* [18–20] and the more realistic *spatial stability analysis* [21,23], whose fundamental difference

*helio@us.es

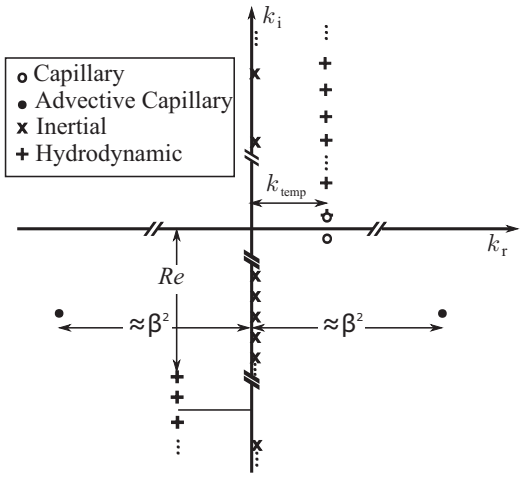

FIG. 1. Sketch of the position of the 3D spatial modes in the k-complex plane for $k_{\text{temp}} < 1$. Except for the dominant capillary mode (circle below the k_r axis), the remaining poles with $k_i < 1$ correspond to modes living upstream.

is the observer's frame of reference, which is solidary to the jet in the former case and to the laboratory in the latter case. Thus, the spatial analysis incorporates advection and leads to (i) natural modes in Doppler-type correspondence with those of the temporal analysis (capillary, hydrodynamic), and (ii) new modes (inertial, advective capillary) leading to nontrivial phenomena, such as the absolute instability responsible for the dripping regime [22,23]. The latter reference definitely clarified previous misconceptions about some of the spatial modes just appealing to the region (upstream or downstream) where each mode is living. This was possible owing to the construction of a Green's function for the spatial scheme, instead of restricting to an analysis of the zeros of the dispersion relation in the complex k plane. A sketch of the 3D spatial modes in the complex k plane similar to that presented in Ref. [23] can be found in Fig. 1 for the sake of future reference. Pole positions depend on the Weber number $\beta^2 \equiv \rho v^2 R/\gamma$, the dimensionless wave number used in the temporal analysis $k_{\text{temp}} \equiv \omega/\beta$, and the Reynolds number Reynolds $\equiv \rho v R/\mu$, where v is the jet velocity, ρ is the liquid density, γ its surface tension, μ its dynamic viscosity and ω is a dimensionless perturbation frequency to be defined in Sec. III.

In the same way, 1D models have been applied to both temporal [7,9] and spatial stability analysis [4,24]. Although the temporal analysis gives consistent correspondences between 3D and 1D modes according to an expansion in powers of k, concerning the spatial analysis, the question is not so closed. Pimbley [4] was the first to apply a 1D model, the inviscid slice model, and lately Bogy [24] did so in the more general viscous case through the Cosserat model. Both of them aimed at a modal formulation of a boundary-value problem for the semi-infinite jet harmonically stimulated at the nozzle. Concerning the inviscid modes, two of them certainly corresponded to the two 3D capillary modes, but the two remaining modes were differently interpreted: Pimbley did not attempt to relate them to any of the remaining families of 3D modes; conversely, Bogy was able to identify them as the first mode of the two infinite families reported in Ref. [21]. Bogy claimed that the lack of correspondence with the 3D outcomes was a serious deficiency of the inviscid slice model. This controversy shows up the need for clarification of the relation between 1D and 3D spatial modes, which is a task now accessible owing to the comprehensive classification of the latter in Ref. [23]. Consideration in this latter reference of an infinite jet, instead of a semi-infinite one, just helps to gain perspective about the physical significance and use of the spatial modes, as some of them are living downwards a perturbation point and some others are living upwards.

We are interested in determining the correspondence between 1D and 3D spatial modes. This tasks requires linearization of these models and the construction of a spatial Green's function analogous to that of Ref. [23]. In this spirit, the linear problem for each of the four 1D models is formulated and solved in Sec. III. In addition, this allows us to analyze in Sec. IV not only the correspondence between 3D and 1D modes, but how well 1D models predict the linear evolution of the jet when subjected to normal and tangential surface stresses, and which are their predictions about the onset of absolute instability [25,26].

II. 1D MODELS WITH EXTERNAL SURFACE STRESSES

Consider a capillary jet with axial symmetry around a line taken as the z axis in cylindrical coordinates. Perturbation (stimulation) can be included in the model through a local application of surface stresses, to be described later. 1D models state as a fundamental guess that all fluid mechanical magnitudes can be expanded in powers of the radial coordinate r. Calling $P(r,z,t)$ the pressure and $U(r,z,t)$ and $W(r,z,t)$ the radial and axial velocities, respectively, we have

$$P(r,z,t) = P_0(z,t) + \tfrac{1}{2}r^2 P_2(z,t) + \cdots, \tag{1}$$

$$W(r,z,t) = W_0(z,t) + \tfrac{1}{2}r^2 W_2(z,t) + \cdots, \tag{2}$$

$$U(r,z,t) = -\tfrac{1}{2}r W_{0z}(z,t) - \tfrac{1}{8}r^3 W_{2z}(z,t) - \cdots, \tag{3}$$

where each z in the subscript of a magnitude means a derivative in this coordinate. The last expansion is the one consistent with a solenoidal velocity field.

The original deduction of the four 1D models that we are considering can be found in García and Castellanos [9]. Our contribution is the inclusion of external surface stresses that we will simply call the normal stress $T_n(z,t)$ and the tangential stress $T_t(z,t)$ (notice that the subscript "t," in roman type, refers to "tangential," not to the temporal variable). With these new inputs the stress balance at the free surface can be written as

$$P\mathbf{e}_n - \mathbf{T}_v \cdot \mathbf{e}_n + T_n\mathbf{e}_n + T_t\mathbf{e}_t = (\nabla \cdot \mathbf{e}_n)\mathbf{e}_n, \tag{4}$$

where $\mathbf{e}_n$ and $\mathbf{e}_t$ are the unit vectors normal and tangential to the free surface, respectively, and $\mathbf{T}_v$ is the viscous stress tensor corresponding to the liquid. In what follows, scalings are chosen to be the radius R for all lengths, the capillary time $t_c \equiv (\rho R^3/\gamma)^{\frac{1}{2}}$ for time, $v_c \equiv R/t_c$ for velocity, and γ/R for pressure and surface stresses. The Ohnesorge number $C \equiv \mu/(\rho R\gamma)^{\frac{1}{2}}$ is the only dimensionless number arising in this formulation. The models are the viscous slice, parabolic, Cosserat, and averaged models, which we now present in turn.

A. Viscous slice model

The relevant magnitudes are the radial position of the free surface, $F(z,t)$, the mean axial velocity in each slice of the jet, $\overline{W}(z,t)$, and the inner pressure evaluated at the free surface, $P_S(z,t)$. $\overline{W}(z,t)$ is equivalent to $W_0(z,t)$ at the order of approximation kept by this model, and so is $P_S(z,t)$ to $P_0(z,t)$.

The kinematic condition is

$$(F^2)_t + (F^2\overline{W})_z = 0, \tag{5}$$

where the subscript t, now in italic, stands for temporal derivatives. From the radial component of the stress balance we have

$$P_S - \boldsymbol{\nabla}\cdot\mathbf{e}_\mathrm{n} + C\overline{W}_z = -T_\mathrm{n} - F_z T_\mathrm{t}. \tag{6}$$

Finally, a combination of the axial momentum equation and the tangential stress balance yields

$$F(W_t + \overline{W}\,\overline{W}_z) = -F\,P_{Sz} + C(6F_z\overline{W}_z + 2F\overline{W}_{zz}) + 2K_\mathrm{n}T_\mathrm{t}, \tag{7}$$

with $K_\mathrm{n} \equiv (1+F_z^2)^{1/2}$. Putting $T_\mathrm{n} = T_\mathrm{t} = 0$ and eliminating P_S from (6), we recover the viscous slice model as presented in García and Castellanos [9]. An important feature of this model is that the radial inertia is not included.

B. Parabolic model

This model retains more variables in the radial expansions (2) and (3), so that the final unknowns are F, W_0, W_2, and P_S as functions of z and t. The equations are

$$F_t + \tfrac{1}{2}FW_{0z} + F_zW_0 + \tfrac{1}{8}F^3W_{2z} + \tfrac{1}{2}F^2F_zW_2 = 0, \tag{8}$$

$$P_S - \boldsymbol{\nabla}\cdot\mathbf{e}_\mathrm{n} + C\big(W_{0z} - \tfrac{1}{2}FF_zW_{0zz} + FF_zW_2 + \tfrac{3}{4}F^2W_{2z}\big) = -T_\mathrm{n} - F_zT_\mathrm{t}, \tag{9}$$

$$W_{0t} + W_0W_{0z} - \left[\frac{F^2}{4}\left(W_{0tz} - \frac{1}{2}W_{0z}^2 + W_0W_{0zz}\right)\right]_z = -P_{Sz} + C\left\{W_{0zz} + 2W_2 - \frac{1}{4}[F^2(W_{0zzz} + 2W_{2z})]_z\right\}, \tag{10}$$

and

$$F^3\big(W_{2t} + W_0W_{2z} + \tfrac{1}{2}W_{0tzz} + \tfrac{1}{2}W_0W_{0zzz}\big) + C\big[4F\big(F_z^2-1\big)(W_{0zz} - 2W_2) - 24F_zW_{0z} - 14F_zF^2W_{2z} - \tfrac{1}{2}F^3W_{0zzzz} - 3F^3W_{2zz}\big] = 8K_\mathrm{n}^2T_\mathrm{t}. \tag{11}$$

The last equation makes the difference with respect to the viscous slice model and comes from a combination of the tangential stress balance and a second-order axial momentum equation. A radial momentum equation is also embedded in the model through the elimination of one of the pressure variables P_0 and P_2, also related through the redefinition $P_S \equiv P_0 + F^2P_2/2$. Again, eliminating P_S from (9) and setting both external stresses to zero yields the parabolic model reported in Ref. [9].

C. Cosserat model

As this model is often considered in the literature [27], we include here their equations, in spite of it being a mean velocity model inconsistently derived from the parabolic model [9]. The relevant magnitudes are the same as in the viscous slice model, although the mean velocity $\overline{W}$ is not equivalent to W_0. The equations, having the same meaning, are

$$(F^2)_t + (F^2\overline{W})_z = 0, \tag{12}$$

$$P_S - \boldsymbol{\nabla}\cdot\mathbf{e}_\mathrm{n} + CG = H, \tag{13}$$

$$F^2(\overline{W}_t + \overline{W}\,\overline{W}_z) - \left[\frac{F^4}{8}\left(\overline{W}_{zt} - \frac{1}{2}\overline{W}_z^2 + \overline{W}\,\overline{W}_{zz}\right)\right]_z + CJ + F^2P_{Sz} = L, \tag{14}$$

where G, H, J, and L are defined as

$$\begin{aligned} G &= \overline{W}_z - \tfrac{1}{2}FF_z\overline{W}_{zz},\\ H &= -T_\mathrm{n} - F_zT_\mathrm{t},\\ J &= F^2\big(F_z^2-2\big)\overline{W}_{zz} - 6FF_z\overline{W}_z + \tfrac{1}{8}(F^4\overline{W}_{zzz})_z,\\ L &= 2FK_n^2T_\mathrm{t}. \end{aligned} \tag{15}$$

D. Averaged model

This model is another mean velocity one, improved with respect to the Cosserat model in that its derivation is carried out in a consistent manner by retaining all terms of the same order [9]. The variables are the same, as well as the structure of the governing equations, up to the point that we have to merely redefine the functions G, H, J, and L in the following form:

$$\begin{aligned} G &= \big(1 + \tfrac{3}{2}F_{zz}F\big)\overline{W}_z + \tfrac{5}{4}F_zF\overline{W}_{zz} + \tfrac{1}{4}F^2\overline{W}_{zzz}\\ H &= -T_\mathrm{n} - T_\mathrm{t}(F_z + FK_{n,z}K_n) - \tfrac{1}{2}FT_{\mathrm{t},z}K_n^2\\ J &= \big(\tfrac{9}{2}FF_z^3 - 6FF_z + \tfrac{3}{4}F^3F_{zzz} + \tfrac{15}{4}F^2F_zF_{zz}\big)\overline{W}_z + \big(2FF_{zz} + \tfrac{7}{2}F_z^2 - 2\big)F^2\overline{W}_{zz} + \tfrac{7}{4}F^3F_z\overline{W}_{zzz} + \tfrac{1}{4}F^4\overline{W}_{zzzz},\\ L &= \big(2FK_n^2 - \tfrac{3}{2}FK_n^2F_z^2 - \tfrac{1}{2}F^3K_{n,z}^2 - \tfrac{1}{2}F^3K_nK_{n,zz} - F^2K_nF_zK_{n,z} - \tfrac{3}{4}F^2K_n^2F_{zz}\big)T_\mathrm{t} - \tfrac{1}{2}F^2\big(FK_n^2\big)_zT_{\mathrm{t},z} - \tfrac{1}{4}F^3K_n^2T_{\mathrm{t},zz}. \end{aligned} \tag{16}$$

Once again, eliminating P_S from these equations yields a reduced system consistent (putting $H = L = 0$) with the averaged model presented in García and Castellanos [9]. However, in the formulation proposed in that reference, the model has a serious drawback which manifests as a numerical instability in the computation of the jet evolution, especially in the final stages of the breakup process, as reported in García [28]. This behavior is there diagnosed as a negative dissipation and cured as well by including in the expression for J some higher-order terms by means of the substitution

$$J \leftarrow J - \tfrac{3}{64}\big[F^2\big(F^2F_{zz}^2 - 6FF_z^2F_{zz} + 9F_z^4\big)\overline{W}_z\big]_z, \tag{17}$$

to make the dissipation function positive definite without changing the order of approximation of the model. Numerical tests confirmed in the above-mentioned reference that the evolution of the jet is virtually the same in the first stages and the scheme becomes stable up to the breakup. Thus, the same recipe must be applied to our extended averaged model.

Note that the averaged model is the only one that requires computation of spatial derivatives of the external stresses T_n and T_t. This fact may make it less attractive than the others.

III. LINEARIZATION AND RESOLUTION

Under the assumption of small effects of a local stimulation on the fluid mechanical magnitudes, we can linearize the above equations for all the models, by applying the substitutions pertinent to each model among

$$\begin{aligned} &\overline{W} = \beta + \overline{w}, \quad W_0 = \beta + w_0, \\ &W_2 = w_2, \quad P_S = 1 + p, \quad F = 1 + f, \end{aligned} \tag{18}$$

and neglecting all the terms with products of the perturbed magnitudes. The parameter $\beta \equiv v/v_c$ is the dimensionless unperturbed jet velocity, i.e., the square root of the Weber number. We assume that the external stresses T_n and T_t dictate the size of the perturbations. For the sake of simplicity of writing, we shall group viscous slice, Cosserat, and averaged models, with common unknowns, in only one set of equations by introducing two parameters, l and s, whose values determine which model we are considering. Their equations are

$$f_t + \beta f_z + \tfrac{1}{2}\overline{w}_z = 0, \tag{19}$$

$$-p - f - f_{zz} - C\left(\overline{w}_z + \tfrac{1}{4}l\overline{w}_{zzz}\right) = T_n, \tag{20}$$

$$\begin{aligned} &\frac{1}{2}\left(\overline{w}_t + \beta\overline{w}_z + p_z\right) - \frac{1}{16}s(\overline{w}_{tzz} + \beta\overline{w}_{zzz}) \\ &\quad + C\left(s\frac{1+l}{16}\overline{w}_{zzzz} - \overline{w}_{zz}\right) = T_t, \end{aligned} \tag{21}$$

from which the linearized viscous slice model is obtained by putting $s = 0$ and $l = 0$, the linearized Cosserat model with $s = 1$ and $l = 0$, and finally the linearized averaged model with $s = 1$ and $l = 1$.

The parabolic model needs a specific set of equations, as their unknowns are different:

$$f_t + \beta f_z + \tfrac{1}{2}w_{0z} + \tfrac{1}{8}w_{2z} = 0, \tag{22}$$

$$-p - f - f_{zz} - C\left(w_{0z} + \tfrac{3}{4}w_{2z}\right) = T_n, \tag{23}$$

$$\begin{aligned} &w_{0t} + \beta w_{0z} + p_z - \tfrac{1}{4}(w_{0tzz} + \beta w_{0zzz}) \\ &\quad - C\left(w_{0zz} + 2w_2 - \tfrac{1}{2}w_{2zz} - \tfrac{1}{2}w_{0zzzz}\right) = 0, \end{aligned} \tag{24}$$

$$\begin{aligned} &w_{2t} + \beta w_{2z} + \tfrac{1}{2}(w_{0tzz} + \beta w_{0zzz}) \\ &\quad + C\left(8w_2 - 4w_{0zz} - 3w_{2zz} - \tfrac{1}{2}w_{0zzzz}\right) = 8T_t. \end{aligned} \tag{25}$$

The next step is the resolution of these linear problems by means of the Green's function formalism. As in Guerrero *et al.* [23], we consider the inputs T_n and T_t as delta functions in the z coordinate, multiplied by a sinusoidal temporal dependence starting at $t = 0$, in order to define the Green's functions for harmonic surface stimulation. The onset of the stimulation at a definite instant guarantees a correct physical formulation from the point of view of causality (signaling problem) [25,26,29]. The resulting solution has a transient part which is decaying unless the jet is absolutely unstable (depending on the nondimensional parameters C and β), and a permanent harmonic response with the same dimensionless angular frequency ω as the stimulation. The relevant part of the solution is, again in the decaying transient case, the harmonic asymptotic response. If we restrict ourselves from the beginning to the asymptotic part of the solution, we can assume a temporal dependence of the form $\exp(i\omega t)$ and perform a Fourier transform only in the spatial coordinate z, for all the unknowns defined in each model. For example, for the viscous slice, Cosserat, and averaged models we define

$$\{\tilde{p}, \tilde{w}, \tilde{f}, \tilde{T}_n, \tilde{T}_t\} \equiv \int_{-\infty}^{\infty} dz\{p, w, f, T_n, T_t\}\exp(-ikz). \tag{26}$$

With the assumed temporal harmonic dependence and the application of the transform in z to Eqs. (19)–(21), we arrive to an algebraic system for the transformed variables,

$$\mathbf{M}\tilde{\mathbf{x}} = \tilde{\mathbf{T}}, \quad \tilde{\mathbf{x}} = \begin{pmatrix} \tilde{p} \\ \tilde{w} \\ \tilde{f} \end{pmatrix}, \quad \tilde{\mathbf{T}} = \begin{pmatrix} 0 \\ \tilde{T}_n \\ \tilde{T}_t \end{pmatrix}, \tag{27}$$

and the coefficients of the matrix $\mathbf{M}$ are

$$\begin{aligned} &m_{11} = 0, \quad m_{12} = ik/2, \quad m_{13} = i(\beta k - \omega), \quad m_{21} = -1, \\ &m_{22} = -ikC(1 - lk^2/4), \quad m_{23} = k^2 - 1, \quad m_{31} = ik/2, \\ &m_{32} = (\beta k - \omega)(1 + sk^2/8)i/2 + C[k^2 + s(1 + l)k^4/16], \\ &m_{33} = 0. \end{aligned} \tag{28}$$

Our deduction, besides including surface stresses in a general way, is also different in retaining the pressure as an explicit unknown. This parallelism with the 3D formulation of Guerrero *et al.* [23] makes our 1D formulations simpler and clearer.

For the parabolic model we have a linear system of four variables,

$$\tilde{\mathbf{x}} = \begin{pmatrix} \tilde{p} \\ \tilde{w}_0 \\ \tilde{w}_2 \\ \tilde{f} \end{pmatrix}, \quad \tilde{\mathbf{T}} = \begin{pmatrix} 0 \\ \tilde{T}_n \\ 0 \\ 8\tilde{T}_t \end{pmatrix},$$

and the coefficients of the matrix $\mathbf{M}$ are

$$\begin{aligned} &m_{11} = 0, \quad m_{12} = ik/2, \quad m_{13} = ik/8, \quad m_{14} = i(\beta k - \omega), \\ &m_{21} = -1, \quad m_{22} = -iCk, \quad m_{23} = -3iCk/4, \\ &m_{24} = k^2 - 1, \quad m_{31} = ik, \\ &m_{32} = [i(\beta k - \omega) + Ck^2](1 + k^2/4), \\ &m_{33} = -C(2 + k^2/2), \quad m_{34} = 0, \quad m_{41} = 0, \\ &m_{42} = -ik^2(\beta k - \omega)/2 + Ck^2(4 - k^2/2), \\ &m_{43} = i(\beta k - \omega) + C(8 + 3k^2), \quad m_{44} = 0. \end{aligned} \tag{29}$$

TABLE I. Spatial modes captured by each 1D model, compared with those of the 3D model. Arrows indicate transformations of modes as the jet velocity diminishes.

Model	Downstream modes	Upstream modes
3D	Capillary (2) Inertial (∞) Hydrodynamic (∞)	Advective capillary (2) Inertial (∞) Hydrodynamic (∞)
Viscous slice	Capillary (2)	Advective capillary (2)
Cosserat	Capillary (2) Inertial $\rightarrow$ hydrodynamic	Advective capillary (upward) Inertial $\rightarrow$ advective capillary (downward)
Averaged	Capillary (2) Inertial $\rightarrow$ hydrodynamic	Inertial $\rightarrow$ advective capillary (downward)
Parabolic	Capillary (2) Inertial Hydrodynamic	Advective capillary (2) Inertial Hydrodynamic

As in the 3D case, the effects of normal and tangential stresses can be separately treated by making $T_t = 0$ and $T_n = 0$, respectively:

$$\begin{pmatrix} \tilde{p}_n \\ \tilde{p}_t \end{pmatrix} = \begin{pmatrix} \{\mathbf{M}^{-1}\}_{12} \\ \{\mathbf{M}^{-1}\}_{13} \end{pmatrix}, \tag{30}$$

$$\begin{pmatrix} \tilde{w}_n \\ \tilde{w}_t \end{pmatrix} = \begin{pmatrix} \{\mathbf{M}^{-1}\}_{22} \\ \{\mathbf{M}^{-1}\}_{23} \end{pmatrix}, \tag{31}$$

$$\begin{pmatrix} \tilde{f}_n \\ \tilde{f}_t \end{pmatrix} = \begin{pmatrix} \{\mathbf{M}^{-1}\}_{32} \\ \{\mathbf{M}^{-1}\}_{33} \end{pmatrix}. \tag{32}$$

The inverse Fourier transform of these expressions give the three magnitudes: pressure, axial velocity, and surface deformation. Furthermore, their residues calculated at the pole defining each mode give the amplitudes of the three magnitudes for that particular mode.

The condition of null determinant of each version of $\mathbf{M}$ leads to the dispersion relation of the corresponding 1D model: (i) viscous slice,

$$k^4 + 6iC\beta k^3 - k^2(1 + 2\beta^2 + 6iC\omega) + 4k\beta\omega - 2\omega^2 = 0; \tag{33}$$

(ii) Cosserat,

$$iCk^5\beta + k^4(4 - \beta^2 - iC\omega) + 2k^3\beta(12iC + \omega) - k^2(4 + 8\beta^2 + 24iC\omega + \omega^2) + 16k\beta\omega - 8\omega^2 = 0; \tag{34}$$

(iii) averaged,

$$\left(1 - \frac{\beta^2}{4}\right)k^4 + \frac{1}{2}\beta k^3(\omega + 12iC) - k^2\left(2\beta^2 + 6iC\omega + \frac{\omega^2}{4} + 1\right) + 4\beta k\omega - 2\omega^2 = 0; \tag{35}$$

(iv) parabolic,

$$\begin{aligned} &Ck^8 + i\beta(1 + 14C^2)k^7 - [3(6\beta^2 - 5)C + i\omega(1 + 14C^2)]k^6 \\ &+ \beta\left[36C\omega + (7 - 4\beta^2 + 96C^2)\right]k^5 \\ &+ [2C(24 - 48\beta^2 - 9\omega^2) + i\omega(12\beta^2 - 7 - 96C^2)]k^4 \\ &+ 4\beta[48C\omega + i(96C^2 - 4\beta^2 - 3\omega^2 - 2)]k^3 \\ &+ 4[i\omega(12\beta^2 + \omega^2 + 2 - 76C^2) - 8C(4\beta^2 + 3\omega^2 + 2)]k^2 \\ &+ 16\beta\omega(16C - 3i\omega)k + 16\omega^2(-8C + i\omega) = 0. \end{aligned} \tag{36}$$

The difference in these equations with respect to the temporal analysis resides in the inclusion of new terms affected by the dimensionless jet velocity β. Previous works on spatial analysis were based on the dispersion relations of the inviscid slice or the Cosserat models; here, we have provided the dispersion relations for all 1D models. However, the most important contribution of this work is that our Green's function formulation for the modal analysis goes beyond these dispersion relations.

The large slenderness hypothesis traduces in the condition $k_r \ll 1$, under which these equations are expected to be accurate. Later, we will discuss their practical range of applicability.

IV. RESULTS

As Eqs. (33)–(36) are algebraic, the finite set of roots for a given real ω is easily obtained, in contrast to the 3D formulation, where we must deal with transcendental relations having an infinite number of roots. In order to classify the results obtained from the 1D models we must recall the spatial modes of the exact 3D formulation. Figure 1 gives a sketch of the distribution of roots of the 3D dispersion relation in the complex k plane, as presented in Guerrero *et al.* [23]. There we can find the roots corresponding to the

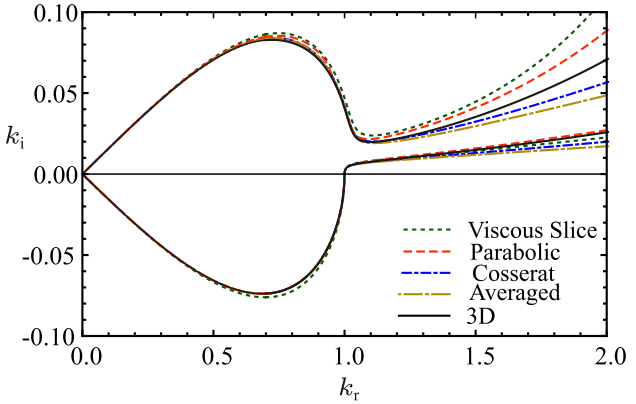

FIG. 2. Dispersion curve of the two capillary modes in the k plane evaluated with 1D and 3D models. The fixed parameters are $C = 0.03$ and $\beta = 4.47$.

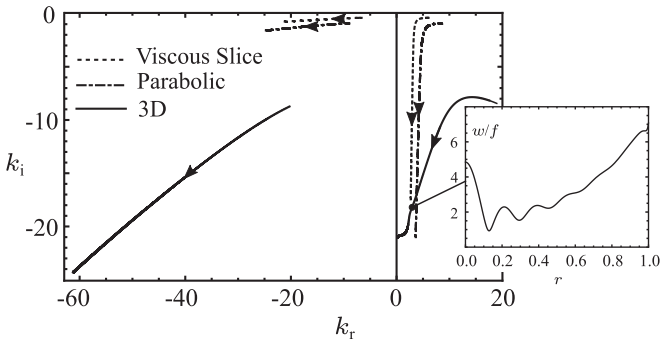

FIG. 3. Dispersion curves (i.e., varying ω) of the two advective capillary modes in the k plane evaluated from 1D (viscous slice and parabolic) and 3D models. The inset shows the axial-velocity profile for the 3D model when the agreement with 1D models about the pole locations is good.

two capillary modes defined downstream, the two advective capillary modes defined upstream, and the two infinite families of hydrodynamic and inertial modes, defined in both regions. Table I presents the modes captured by each model, along with those of 3D calculations.

The number of modes for each model varies according to degree of the corresponding polynomial dispersion relation. The existence of two well-known capillary modes downstream is predicted by all four models: the subdominant capillary mode, stable for any value of the imposed (real) frequency ω, and the dominant capillary mode, unstable for $\omega < 1$. The remaining families of modes are differently captured by each 1D model. As expected, the most refined one, the parabolic model, with eight roots, yields the most accurate description, adding to the capillary modes the two advective capillary modes defined upstream and one inertial and one hydrodynamic mode in each region. The viscous slice model only adds the two advective capillary modes; the Cosserat model adds the upward advective capillary mode and two inertial modes, each defined in a different region; finally, the averaged model gives this same result except for the omission of the upward advective capillary mode.

From a practical point of view, the dominant capillary mode is the most important one, as it is unstable in the mentioned frequency range and determines the breakup length. A quantitative test of the performance of the various 1D models is their prediction of the spatial growth rate of this mode as compared with the exact result of the 3D model. This is shown in Fig. 2, where we can observe the good agreement of all 1D models in the unstable range. For $k_r > 1$ differences become increasingly bigger. For this range, the parabolic model gives similar results than the Cosserat or the averaged models due to having the same order in k, in spite of the former being algebraically more involved.

A quantitative comparison of predictions of 1D models for other modes, relative to the exact 3D results, gives a poor agreement, as shown in Fig. 3 for the two advective capillary

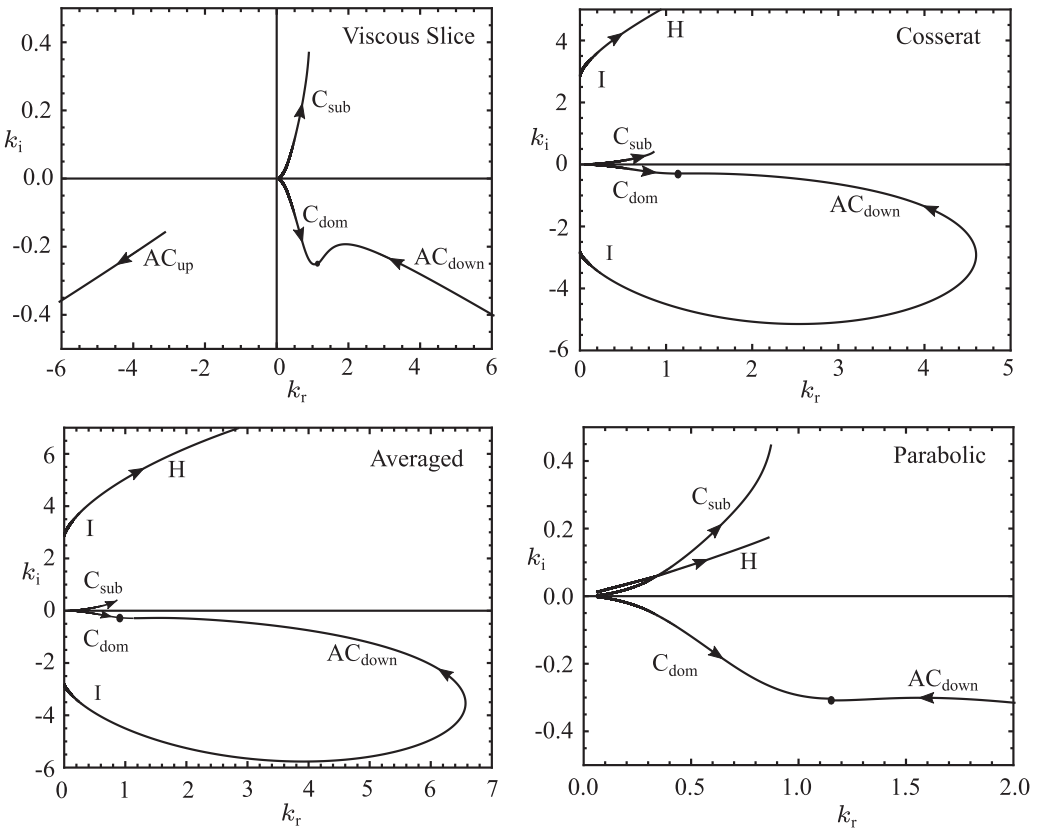

FIG. 4. Movement of modes in the k plane as the jet velocity diminishes from $\beta = 20$ up to the critical velocity β_c for each model. Not all the modes are represented, except for the viscous slice and averaged models. The Ohnesorge number is set to $C = 0.03$ and the dimensionless frequency to the critical value for each model.

modes. The key feature is again a wave number much greater than unity, which violates the assumption made to derive the 1D models. Note that an increase of the frequency results in a decrease of k_r for the roots with a positive value of this parameter and, at the same time, in a migration of these roots to the region of the complex k plane where the 3D root is. The inset of the same figure shows the radial profile of the axial velocity of the downward advective capillary mode. This profile has been computed from the 3D model at a frequency for which the 1D models capable to capture it give similar k-plane locations. Although the profile is still far from uniform nor parabolic, we must recall that the axial velocity of these modes for moderate frequency are strongly nonuniform and typically nonzero only near the free surface [23].

The enumeration made in Table I shows, by means of arrows, transformations of modes taking place as the jet velocity diminish. For the Cosserat and the averaged models, the upstream inertial mode moves gradually to a region where it should rather be considered as the downward advective capillary mode, as shown in Fig. 4. In the same figure we can also observe in both models a change of a downstream inertial mode to somewhat similar to a hydrodynamic mode.

The 3D spatial modes that coalesce in the complex k plane and lead to an absolute instability of the jet are the dominant capillary mode and the downward advective capillary mode, as demonstrated in Guerrero *et al.* [23]. The procedure was to keep the track of these spatial modes as we diminish the jet velocity until coalescence in marginal stability conditions (the frequency is purely real). As these two modes are present in all four 1D models (always in the viscous slice and parabolic models and for low jet velocities in the averaged and Cosserat models), it is not surprising that they also predict the absolute instability. In fact, in Fig. 4 the frequencies for each 1D model have been selected as those leading to marginal absolute instability as the jet velocity diminishes towards its critical value. In this way, we can determine for each model the critical jet velocity β_c as a function of the Ohnesorge number

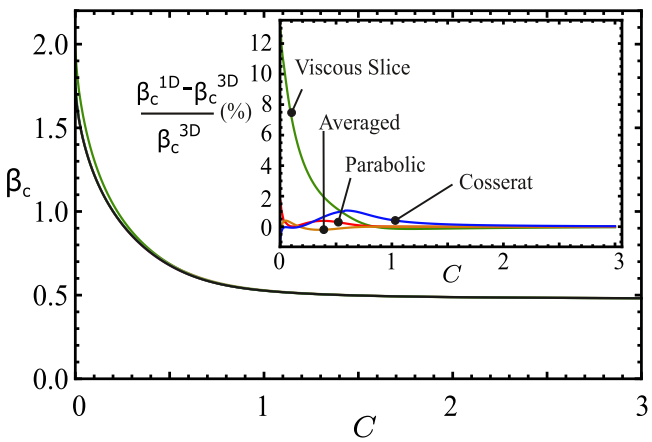

FIG. 5. Absolute-convective instability transition curve in the parameter plane β-C, as predicted by 3D and 1D models. Only the curve obtained from the viscous slice model is distinguishable (the upper one) from that of the 3D model. The inset shows the relative deviation (in percent) of the critical dimensionless velocity given by each 1D model.

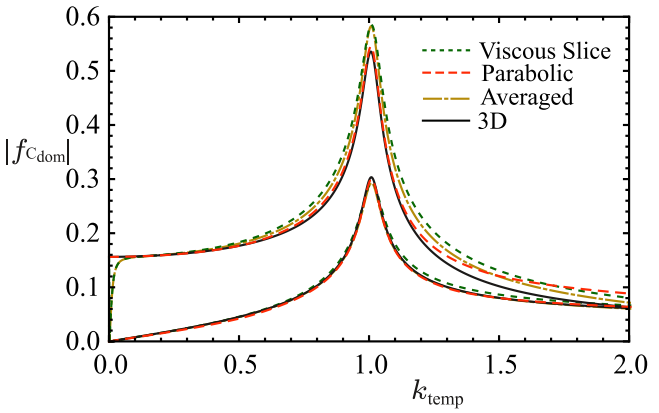

FIG. 6. Amplitude of the contribution of the dominant capillary mode to the surface deformation, computed with 3D and 1D models. The upper family of curves corresponds to tangential stress stimulation. The averaged model (present) and the Cosserat model (omitted) give indistinguishable curves.

C in an equivalent manner as Leib and Goldstein [22] did for the critical Weber number We_c as a function of the Reynolds number Re. This classical curve is reproduced, labeled as 3D, in Fig. 5 in terms of our preferred parameters β and C, along with the predictions of the 1D models. The agreement is within a 1% of relative deviation, except for the viscous slice model and $C \to 0$, for which the relative deviation increases as C decreases until some 13% for $C = 0$ (specifically, $\beta_c = 2$ for the viscous slice model and $\beta_c = \sqrt{\pi}$ for the 3D model).

Besides the complex wave number of each spatial mode, the information extracted from the Green's function formalism is the receptivity of the system, intended as the amplitude of each mode, obtained from Eqs. (30)–(32) by a residue calculation. Figure 6 presents the one of the dominant capillary mode for normal and tangential stresses for the 3D and the four 1D models. The agreement is quite good, although much better for normal stress. As in 3D computations, the conclusion is that tangential stress stimulation is more effective than normal stress stimulation, for the same applied force per unit area.

V. DISCUSSION

1D models have been extended in Sec. II to account for any physical mechanism acting on the jet through surface stress as an input. Many applications are envisaged: EHD stimulation, action of magnetic fields on magnetizable fluids, thermocapillary stimulation, surfactant effects, etc. Owing to the nature of 1D models, only axisymmetric forces can be considered. As an example, the effect of transversal electric fields is outside the capabilities of these extended models. Another requirement to have in mind is the uncoupling of the outer fluid with the liquid jet. Otherwise, the surface stresses would not be inputs but unknowns of the problem. An example of this kind of restriction is the flow-focusing configuration [30], for which these models are not applicable.

We are now interested in clarifying the use of 1D models done by previous authors in the light of the outcomes presented in Sec. IV. As mentioned in the Introduction, both Pimbley [4] through the inviscid slice model and Bogy [7] through the

Cosserat model tried to describe the spatial evolution of capillary jets issuing from a nozzle at which some boundary conditions over deformation and axial velocity (semi-infinite jet) were imposed. In the first case, the inviscid slice model predicts four modes. Accordingly, Pimbley proposed four boundary conditions at the exit: three over the deformation and some z derivatives and one over the axial velocity. These conditions were not adequately justified. By inspecting Table I we can observe that the viscous slice model only yields two downward modes, so the two natural conditions over the deformation and axial velocity are enough to formulate the boundary-value problem.

In the second case, Bogy used the Cosserat model and found the five modes appearing in Table I. For the boundary-value problem formulation, he restricted himself to inviscid jets, having only four modes (the upward advective capillary mode disappears in that case). He gave radiation-condition arguments to discard one mode that we identify as the upstream inertial mode (highly unstable if incorrectly considered as living downstream) and simply dropped the other present inertial mode because it is the complex conjugate of the former, not a convincing argument. In this way, he finally retained the two capillary modes to formulate the boundary-value problem. Now we can give an alternative formulation by selecting only the downstream modes of Table I corresponding to the Cosserat model. Note that besides the two capillary modes, we must retain one inertial mode, the one with a strong decay. In order to discard this inertial mode, which is the sole member of the infinite family of inertial 3D spatial modes, we have to recall that such modes, as well as those of the hydrodynamic family, should be retained for a more general boundary-value problem having radial dependence of the velocity profile at the jet exit. For a jet with a plug profile at the exit, only the two capillary modes are necessary to formulate the problem, in a similar way as the initial-value problem of the temporal analysis carried out in Ref. [20]. We want to remark the importance of being acquainted to the 3D spatial modal analysis in order to correctly interpret the 1D findings.

Throughout the previous section we have established the general idea of a good performance of all 1D models whenever a specific feature of the exact 3D outcomes fits the requirement $k_r \ll 1$. Evidences sustaining this assertion are as follows: (i) the accurate 1D estimates of the growth rate of the dominant capillary mode in the unstable range $0 < k_r < 1$ and the increasing deviation for increasing k_r beyond this range; (ii) the poor estimates of other modes with $k_r \gg 1$ such as the advective capillary modes; (iii) the approaching to the 3D value of the upward advective capillary mode when the spatial branch obtained by increasing ω reduces the value of k_r; (iv) the good agreement of all predictions about the onset of absolute instability because of the merging of complex k roots at moderate values of k_r; and (v) the good agreement of the amplitude of the dominant capillary mode in the unstable range and its increasing deviation with k_r for $k_r > 1$. Accordingly, we must be careful when dealing with 1D models in applications involving modes with large wave numbers.

Besides the resulting number of modes, the other feature of 1D models that can play a role in their performance is their description of the velocity field. The viscous slice model discards radial inertia, so it is not surprising that this model does not predict the existence of inertial modes, just the ones involving a competition between axial and radial inertia [23]. The remaining 1D models take into account the radial inertia, and their associated dispersion relations yield roots that can be interpreted as corresponding to an inertial mode.

In the same line, the capture of the hydrodynamic modes needs a modelization of the velocity field less simplified than the uniform axial-velocity profile associated with the viscous slice model. The actual profiles obtained through the 3D model for the two infinite families of hydrodynamic modes are essentially recirculating, with almost null mean axial velocity, and a number of internal rolls in the radial direction equal to the family index [23]. The parabolic model, so named due to its radial dependence of the axial-velocity profile, is better suited and indeed it qualitatively predicts the existence of the first hydrodynamic mode of each 3D infinite family.

Another issue for which the velocity profile of 1D models determines their performance is in the evaluation of the amplitude of the dominant capillary mode, illustrated in Fig. 6. A tangential stress implies a transfer of axial momentum from the free surface to the bulk of the jet, so the velocity profile is not uniform. This is in contrast with the application of a normal stress, for which the axial momentum is transferred essentially in a uniform manner to the bulk. As a consequence, the agreement with the exact 3D curves is better for radial stresses than for tangential ones. Again, the more sophisticated velocity description of the parabolic model gives the best outcomes in the description of tangential stress stimulation.

The good results of 1D models in the analysis of the jet pinch-off [31], where higher harmonics significantly grow from nonlinear interactions between modes, is surprising. However, the absence of important nonuniformities in the velocity field may explain this success. On the other hand, the study of imperfectly conducting jets subjected to electrical stresses, carried out by López-Herrera *et al.* [15] for 1D and 3D models, allows us to assess the performance of the formers when the axial velocity has strong nonuniformities: In the limit of very low viscosities, the tangential electric stress is balanced in a viscous boundary layer adjacent to the free surface. As expected, only the parabolic model shows similar results as the exact 3D calculations, provided that viscosity is not too low.

VI. CONCLUSIONS

The recent knowledge of the full set of spatial modes of capillary jets gives us the opportunity to test the performance of 1D models in reproducing 3D results and, at the same time, in clarifying the first attempts of application of 1D models to the spatial problem, found in the literature. To this end, the existing formulations of four 1D models (viscous slice, averaged, Cosserat, and parabolic) have been adapted to deal with jets described from the laboratory framework and subjected to tangential and normal stresses on its surface.

The accuracy of 1D models is consistently related to the size of the nondimensional wave number involved in each phenomenon. We have reported the failure of these models to describe modes with intrinsically large wave numbers, namely, the advective capillary modes. Conversely, they succeed in

describing the absolute instability threshold or the growth rate and amplitude of the dominant capillary mode resulting from surface stress stimulation, i.e., two phenomena with moderate wave numbers.

The other ingredient in evaluating the performance of each 1D model is the ability to deal with nonuniform velocity-profile situations. The parabolic model, although slightly costlier, is more suited to these applications, as illustrated in the capture of hydrodynamic spatial modes or in the evaluation of the amplitude of the dominant capillary mode as a response to a tangential stress stimulation.

ACKNOWLEDGMENTS

This work was supported by the Spanish Government under Contract No. FIS2011-25161 and by the Junta de Andalucía under Contract No. P11-FQM-7919.

[1] C. Weber, Z. Angew. Math. Mech. **11**, 136 (1931).
[2] J. R. Melcher and E. P. Warren, J. Fluid Mech. **47**, 127 (1971).
[3] H. C. Lee, IBM J. Res. Dev. **18**, 364 (1974).
[4] W. T. Pimbley, IBM J. Res. Dev. **20**, 148 (1976).
[5] A. E. Green, Int. J. Eng. Sci. **14**, 49 (1976).
[6] D. W. Bousfield, R. Keunings, G. Marrucci, and M. M. Denn, J. Non-Newtonian Fluid Mech. **21**, 79 (1986).
[7] D. B. Bogy, Phys. Fluids **21**, 190 (1978).
[8] J. Eggers and T. F. Dupont, J. Fluid Mech. **262**, 202 (1994).
[9] F. J. García and A. Castellanos, Phys. Fluids **6**, 2676 (1994).
[10] M. Rubio-Rubio, A. Sevilla, and J. M. Gordillo, J. Fluid Mech. **729**, 471 (2013).
[11] F. J. García, H. González, J. R. Castrejón-Pita, and A. A. Castrejón-Pita, Appl. Phys. Lett. **105**, 094104 (2014).
[12] M.-L. E. Timmermans and J. R. Lister, J. Fluid Mech. **459**, 289 (2002).
[13] D. W. Hrdina and J. M. Crowley, IEEE Trans. Ind. Appl. **25**, 705 (1989).
[14] B. Barbet, Ph.D. thesis, Université Joseph Fourier, Grenoble 1, France, 1997.
[15] J. M. López-Herrera, P. Riesco-Chueca, and A. M. Gañán Calvo, Phys. Fluids **17**, 034106 (2005).
[16] S. N. Reznik and E. Zussman, Phys. Rev. E **81**, 026313 (2010).
[17] E. P. Furlani, J. Phys. A **38**, 263 (2005).
[18] L. Rayleigh, Proc. London Math. Soc. **10**, 4 (1878).
[19] L. Rayleigh, Philos. Mag. **34**, 145 (1892).
[20] F. J. García and H. González, J. Fluid Mech. **602**, 81 (2008).
[21] J. B. Keller, S. I. Rubinow, and Y. O. Tu, Phys. Fluids **16**, 2052 (1973).
[22] S. J. Leib and M. E. Goldstein, Phys. Fluids **29**, 952 (1986).
[23] J. Guerrero, H. González, and F. J. García, J. Fluid Mech. **702**, 354 (2012).
[24] D. B. Bogy, Trans. ASME **45**, 469 (1978).
[25] P. Huerre and P. A. Monkewitz, Annu. Rev. Fluid Mech. **22**, 473 (1990).
[26] J. M. Gordillo and M. Pérez-Saborid, Phys. Fluids **14**, 4329 (2002).
[27] D. B. Bogy, Annu. Rev. Fluid Mech. **11**, 207 (1979).
[28] F. J. García, Ph.D. thesis, Universidad de Sevilla, 1998.
[29] N. S. Barlow, S. J. Weinstein, and B. T. Helenbrook, J. Fluid Mech. **699**, 115 (2012).
[30] A. M. Gañán-Calvo, Phys. Rev. Lett. **80**, 285 (1998).
[31] B. Ambravaneswaran, E. D. Wilkes, and O. A. Basaran, Phys. Fluids **14**, 2606 (2002).